



11 Antiproton over proton and K^- over K^+ multiplicity ratios at high z in 12 DIS

13 The COMPASS Collaboration

14 ARTICLE INFO

15 Article history:

21 Received 5 April 2020

22 Received in revised form 26 June 2020

23 Accepted 28 June 2020

24 Available online xxxx

25 Editor: L. Rolandi

26 Keywords:

27 Quantum chromodynamics

28 pQCD

29 Deep-inelastic scattering

30 Hadron multiplicities

31 COMPASS

16 ABSTRACT

17 The antiparticle-over-particle multiplicity ratio is measured in deep-inelastic scattering for negatively and
18 positively charged kaons and, for the first time, for antiprotons and protons. The data were obtained by
19 the COMPASS Collaboration using a 160 GeV muon beam impinging on an isoscalar ^6LiD target. The
20 regime of deep-inelastic scattering is ensured by requiring $Q^2 > 1 \text{ (GeV/c)}^2$ for the photon virtuality and
21 $W > 5 \text{ GeV/c}^2$ for the invariant mass of the produced hadronic system. Bjorken- x is restricted to the
22 range 0.01 to 0.40. Protons and antiprotons are identified in the momentum range from 20 GeV/c to 60
23 GeV/c and required to carry a large fraction of the virtual-photon energy, $z > 0.5$. In the whole studied
24 z -region, the \bar{p} over p multiplicity ratio is found to be below the lower limit expected from calculations
25 based on leading-order perturbative Quantum Chromodynamics (pQCD). Kaons were previously analysed
26 in the momentum range 12 GeV/c to 40 GeV/c. In the present analysis this range is extended up to
27 55 GeV/c, whereby events with larger virtual-photon energies are included in the analysis and the
28 observed K^- over K^+ ratio becomes closer to the expectation of next-to-leading order pQCD. The results
29 of both analyses strengthen our earlier conclusion that at COMPASS energies the phase space available
30 for single-hadron production in deep-inelastic scattering should be taken into account in the standard
31 pQCD formalism.

32 © 2020 Published by Elsevier B.V. This is an open access article under the CC BY license
33 (<http://creativecommons.org/licenses/by/4.0/>). Funded by SCOAP³.

34 **1. Introduction**

35 Within the standard approach of perturbative Quantum Chromodynamics (pQCD), hadron production from an active quark in
36 a deep-inelastic scattering process (DIS) is effectively described
37 by non-perturbative objects called fragmentation functions (FFs). These functions presently cannot be predicted by theory, but their
38 scale evolution is described by the DGLAP equations [1]. For a given negative four-momentum transfer squared Q^2 , in leading
39 order (LO) pQCD the FF $D_q^h(z, Q^2)$ represents the probability density that a hadron h is produced in the fragmentation of a quark
40 with flavour q . The produced hadron carries a fraction z of the virtual-photon energy ν , where the latter is defined in the laboratory
41 frame.

42 The cleanest way to access FFs consists in studying single-inclusive hadron production in lepton annihilation, $e^+ + e^- \rightarrow h + X$, where the remaining final state X is not analysed. However, only information about $D_q^h + D_{\bar{q}}^h$ is accessible there and only limited flavour separation is possible. Additional input, like semi-inclusive measurements of deep-inelastic lepton-nucleon scattering (SIDIS), is required to fully understand quark fragmentation into hadrons. In the case of the SIDIS cross section, FFs are convoluted with parton distribution functions (PDFs). As these are rather well known, FFs for q and \bar{q} can be accessed separately and full flavour separation is possible in principle. As a result, FFs obtained using

43 only e^+e^- data differ in some cases significantly from those that
44 were determined by additionally taking into account data from
45 SIDIS or other processes, see Refs. [2–7].

46 Recently, the HERMES and COMPASS Collaborations have published several papers concerning unidentified hadron, pion and
47 kaon multiplicities in SIDIS, see Refs. [8–11]. In the most recent
48 COMPASS article [12] it was shown that for kaons at high z the
49 K^- over K^+ multiplicity ratio R_K falls below the lower limit predicted by pQCD. From the measured ν -dependence it was concluded
50 that in experiments with similar (or lower) centre-of-mass energy than COMPASS an insufficient description of the data by
51 pQCD may affect the region of high and also medium values of z . These kinematic regions are important in many respects, as e.g. transverse-momentum-dependent azimuthal asymmetries are quite pronounced there [13]. Hence the above described phenomenon should be better understood in order to avoid possible bias when extracting FFs and/or transverse-momentum-dependent PDFs and FFs by applying the standard pQCD formalism to SIDIS data in these regions.

52 In order to provide more experimental results for further phenomenological studies, we present here for the first time the COMPASS results on the \bar{p} over p multiplicity ratio R_p at high z , i.e. $z > 0.5$, which are obtained from SIDIS data taken on an isoscalar target. In addition we present new results on R_K , obtained in a ν -range extended with respect to Ref. [12], which became attain-

53 <https://doi.org/10.1016/j.physletb.2020.135600>

54 0370-2693/© 2020 Published by Elsevier B.V. This is an open access article under the CC BY license (<http://creativecommons.org/licenses/by/4.0/>). Funded by SCOAP³.

able by improving the kaon identification procedure. Note that when measuring a multiplicity ratio, several systematic uncertainties cancel in both theory and experiment. Thus a multiplicity ratio can be considered as one of the most robust observables presently available when analysing SIDIS data and the analysis given in this Letter hence presents a test of the applicability of pQCD in the studied kinematic domain.

This Letter is organised as follows. In Section 2, pQCD-based predictions for R_p and R_K are discussed. Experimental set-up and data selection are described in Section 3. The analysis method is presented in Section 4, followed by the discussion of systematic uncertainties in Section 5. The results are presented and discussed in Section 6.

2. Theoretical framework and model expectations

Hadrons of type h produced in the final state of DIS are commonly characterised by their relative abundance. The hadron multiplicity M^h is defined as ratio of the SIDIS cross section for hadron type h and the cross section for an inclusive measurement of the deep-inelastic scattering process (DIS):

$$\frac{dM^h(x, Q^2, z)}{dz} = \frac{d^3\sigma^h(x, Q^2, z)/dxdQ^2dz}{d^2\sigma^{\text{DIS}}(x, Q^2)/dxdQ^2}. \quad (1)$$

Here, x denotes the Bjorken scaling variable. The cross sections σ^{DIS} and σ^h can be composed using the standard factorisation approach of pQCD [14,15]. In the following, the LO pQCD expressions for the cross section calculations will be used. In the LO approximation for the multiplicity, where the sum over parton species $a = q, \bar{q}$ is weighted by the square of the electric charge e_a of the quark expressed in units of the elementary charge, only simple products of PDFs $f_a(x, Q^2)$ and FFs $D_a^h(z, Q^2)$ are involved instead of the aforementioned convolutions:

$$\frac{dM^h(x, Q^2, z)}{dz} = \frac{\sum_a e_a^2 f_a(x, Q^2) D_a^h(z, Q^2)}{\sum_a e_a^2 f_a(x, Q^2)}. \quad (2)$$

For a deuteron target, the \bar{p} over p multiplicity ratio in LO pQCD reads as follows:

$$\begin{aligned} R_p(x, Q^2, z) &= \frac{dM^{\bar{p}}(x, Q^2, z)/dz}{dM^p(x, Q^2, z)/dz} \\ &= \frac{4.5(\bar{u} + \bar{d})D_{\text{fav}} + (5u + 5d + 2s + 2\bar{s})D_{\text{unf}}}{4.5(u + d)D_{\text{fav}} + (5\bar{u} + 5\bar{d} + 2s + 2\bar{s})D_{\text{unf}}}. \end{aligned} \quad (3)$$

Here, $u, \bar{u}, d, \bar{d}, s, \bar{s}$ denote the PDFs in the proton for corresponding quark flavours. Their dependences on x and Q^2 are omitted for brevity. The symbols D_{fav} (D_{unf}) denote favoured (unfavoured) FFs and their dependence on z and Q^2 are also omitted for brevity. Presently, proton FFs and their ratios are not well known at high z as their extraction is based on e^+e^- annihilation data only [2]. Following Refs. [2] and [16] it is assumed that $D_u^p = 2D_d^p = D_{\text{fav}}$. In addition, the existing data do not allow to distinguish between different functions D_{unf} for different quark flavours. In the large- z region, the ratios $D_{\text{unf}}/D_{\text{fav}}$ are expected to be small.¹ Neglecting D_{unf} in Eq. (3) leads to the following lower limit for R_p in LO pQCD:

$$R_p > \frac{\bar{u} + \bar{d}}{u + d}. \quad (4)$$

¹ For kaons, this expectation is indeed confirmed in pQCD fits already at moderate values of z , see e.g. Ref. [6].

It depends only upon rather well known PDFs and is independent on the assumption $D_u^p = 2D_d^p = D_{\text{fav}}$. It is interesting to note that the lower limit predicted by LO pQCD is the same for both protons and kaons [12], while in general $R_K > R_p$ is expected as in the case of kaons strange quark FFs ($D_s^{K^-}, D_{\bar{s}}^{K^+}$) are involved, which are of the favoured type contrary to the proton case.

The present analysis is performed in two x -bins, below and above $x = 0.05$. The average values of x and Q^2 are $\langle x \rangle = 0.023$, $\langle Q^2 \rangle = 2.4 \text{ (GeV/c)}^2$ in the first x -bin and $\langle x \rangle = 0.10$, $\langle Q^2 \rangle = 9.8 \text{ (GeV/c)}^2$ in the second one. Based on Eq. (4) and the MSTW08LO PDF set from Ref. [17], the expected lower limits on R_p in these two x -bins are 0.51 and 0.28. These values are about 10% higher if newer PDF sets as in Refs. [18,19] are used instead. Due to the above mentioned lack of reliable proton FFs at NLO, presently no predictions can be made for the lower limit of R_p at higher perturbative order.

We also evaluate R_p with the LEPTO Monte Carlo event generator [20] (version 6.5), with the result that the LUND string fragmentation model [21] used in LEPTO is incapable to model R_p correctly. For example, for $z = 0.5$ LEPTO predicts $R_p \approx 1$, which is definitely not supported by the data as it will be shown below. On the other hand, for $z > 0.85$ the predicted value of R_p falls below the LO pQCD lower limit. This is possible as in the LUND model the mechanism of string hadronisation does not only depend on quark and hadron types and on z , as in pQCD, but also on the type of the target nucleon and on x , see Ref. [22] for more details.

Due to different lower momentum limits for particle identification at COMPASS, 18 GeV/c for protons and 9 GeV/c for kaons, the observed x and Q^2 distributions are slightly different for protons and kaons. As a result, the lower limit on R_K is about 0.47, which is obtained for $\langle x \rangle = 0.03$ and $\langle Q^2 \rangle = 1.6 \text{ (GeV/c)}^2$. The LO pQCD predictions for the lower limit on R_K are v independent, because they depend on PDFs in the same way as given in Eq. (4) for the proton case. However, in our earlier measurement [12] a clear v dependence was observed. With higher values of v accessible in the current measurement, we expect the results to be in better agreement with the expectation of (N)LO pQCD. We also note that the NLO lower limit for R_K turns out to be 10%–15% smaller than the LO pQCD lower limit given above, see Ref. [12].

Some phenomenological models [23–25] are able to accommodate R_K below the pQCD limits presented above, but the predicted effect is too small to explain our earlier published results [12]. There are also important theoretical efforts ongoing to improve the formalism (higher-order corrections, treatment of heavy quarks etc.), see e.g. Refs. [26–31], which however do not affect the interpretation of the data shown in Ref. [12] and in the present paper.

3. Experimental set-up and data selection

The present analysis is based on COMPASS data taken in 2006. The 160 GeV/c μ^+ beam delivered by the M2 beam line of the CERN SPS had a momentum spread of about 5%. The beam was naturally polarised, but the polarisation is not affecting this analysis since we integrate over azimuthal angle and transverse momentum of the produced hadrons. The ${}^6\text{LiD}$ target has a total length of 120 cm, which corresponds to about half of a hadron interaction length. It is considered to be isoscalar, and the 0.2% excess of neutrons over protons due to the presence of additional material in the target (${}^3\text{He}$ and ${}^7\text{Li}$) is neglected. The target was longitudinally polarised, but in the present analysis the data are averaged over the target polarisation, which leads to a remaining average target polarisation below 1%.

The COMPASS two-stage spectrometer has a polar angle acceptance of ± 180 mrad, and it is capable of detecting charged particles with momenta as low as 0.5 GeV/c. However, in this analysis typical particle momenta are above 20 GeV/c. The ring-imaging

Cherenkov detector (RICH) was used to identify pions, kaons and protons. Its radiator volume was filled with C_4F_{10} leading to a threshold for pion, kaon and proton identification of about 3 GeV/c , 9 GeV/c and 18 GeV/c respectively. Two trigger types are used in the analysis. The “inclusive” trigger is based on a signal from a combination of hodoscope signals caused by the scattered muon. The “semi-inclusive” trigger requires an energy deposition in one of the hadron calorimeters. The experimental set-up is described in more detail in Ref. [32].

The data selection criteria are kept similar to those used in the recently published analyses [10,12] whenever possible. In order to formally ensure the applicability of the pQCD formalism, the DIS region is selected by requiring $Q^2 > 1 (GeV/c)^2$ and $W > 5 GeV/c^2$ for the invariant mass of the produced hadronic system. The fraction of the incoming muon energy carried by the virtual photon, y , is kept larger than 0.1 to avoid the region with degraded momentum resolution.

For the proton multiplicity analysis, the constraint $x > 0.01$ is used in order to make the kinematic coverage more similar to that of our earlier kaon studies [12]. In the present analysis, we study protons carrying a large fraction z of the virtual-photon energy, $z > 0.5$. In order to ensure efficient proton identification by the RICH, only events with proton momentum above 20 GeV/c are used, i.e. 2 GeV/c above the RICH proton threshold. The upper limit for proton identification is set to 60 GeV/c . Purity and efficiency of the proton selection are optimised by imposing appropriate constraints on the likelihoods of proton, kaon, pion and background hypotheses that are calculated by the RICH particle-identification software [33].

In our earlier studies of R_K [12], kaons with momenta between 12 GeV/c and 40 GeV/c were analysed for $z > 0.75$. By the improvements in the RICH particle-identification software described in Section 4, the momentum range extends now up to 55 GeV/c , which leads to a significant extension of the available v range. All other kaon selection criteria remain unchanged with respect to the earlier analysis.

4. Analysis method

The proton (kaon) multiplicities $M^{p(K)}(x, Q^2, z)$ are determined from the proton (kaon) yields $N^{p(K)}$ normalised by the number of DIS events, N^{DIS} , and corrected by the acceptance $A^{p(K)}(x, Q^2, z)$:

$$\frac{dM^{p(K)}(x, Q^2, z)}{dz} = \frac{1}{N^{DIS}(x, Q^2)} \frac{dN^{p(K)}(x, Q^2, z)}{dz} \frac{1}{A^{p(K)}(x, Q^2, z)}. \quad (5)$$

As in our earlier kaon analysis [12], we use “semi-inclusive” triggers. This is possible because a bias-free determination of N^{DIS} is not needed, as the latter cancels in R_p and R_K . The total number of protons and anti-protons used in the analysis is about 50 000. In addition to about 64 000 kaons analysed in Ref. [12], there are about 13 000 kaons more in the newly explored kinematic range. Note that the kinematic range for protons is wider than that for kaons.

As it was mentioned in Section 2, the proton analysis is performed in two x -bins, below and above $x = 0.05$. In each x -bin, nine bins are used in the reconstructed z variable z_{rec} , with the bin limits 0.50, 0.55, 0.60, 0.65, 0.70, 0.75, 0.80, 0.85, 0.90 and 1.10. In addition, for events in the first x -bin the data are separated in four bins of proton momentum p_h , with the bin limits 20 GeV/c , 30 GeV/c , 40 GeV/c , 50 GeV/c and 60 GeV/c . This 2-dimensional binning allows implicit studies of the v -dependence of R_p . For the second x -bin, the anti-proton statistics is too limited to perform the analysis in the additional dimension of (anti-)proton momentum. For kaons the present analysis is only performed for $x < 0.05$, using five z -bins with bin limits 0.75, 0.80, 0.85, 0.90, 0.95 and

1.05, and five momentum bins with bin limits 30 GeV/c , 35 GeV/c , 40 GeV/c , 45 GeV/c , 50 GeV/c and 55 GeV/c .

In order to determine the multiplicity ratio R_p from the raw yield of \bar{p} and p , only a few correction factors have to be taken into account. First, the correction related to RICH efficiencies is applied. From an analysis of Λ^0 and $\bar{\Lambda}^0$ decays into an (anti-)proton-pion pair it was concluded that the RICH efficiency for p is charge-symmetric within a precision of about 1%. The proton selection, which was improved with respect to our earlier papers, ensures that the contamination from π and K can be safely neglected. Upper limits to such a possible contamination are taken into account in the systematic uncertainty. The acceptance correction factors A^p for p and \bar{p} are determined using Monte Carlo simulations. The same unfolding method is used as in Ref. [12], i.e., in a given (x, Q^2) bin we calculate the ratio of the number of reconstructed events to that of generated ones. Note that in order to count generated (reconstructed) events, generated (reconstructed) variables are used. As for z unfolding, we present the results as a function of z_{corr} , which denotes the value of z reconstructed in the experiment, corrected by the average difference between the generated and reconstructed values of z_{rec} , where the latter are determined by Monte Carlo simulations. The average acceptance ratio for the first x -bin is $A_{\bar{p}}/A_p = 0.912 \pm 0.004$ (stat.) and a similar value is obtained for the second x -bin. The systematic uncertainty related to the acceptance ratio is discussed in the next section. It is also verified by using the DJANGOH Monte Carlo generator [34] that in the COMPASS kinematics the radiative correction for positive and negative particles is of the same value within uncertainties, thus it cancels in the ratio.

Compared to the above proton analysis and the kaon analysis presented in Ref. [12], the raw K^\pm yields are obtained in a different way, which is described below. After that, the present analysis follows closely the same procedure as in the case of the proton analysis and the one from Ref. [12]. With respect to the proton analysis described above it is in addition verified using simulations that the contamination from diffractive vector meson decays (e.g. $\phi \rightarrow K^+K^-$) and charm meson decays is negligible.

In the proton analysis and in the kaon analysis from Ref. [12], the raw yields are obtained directly by counting the number of events that fulfil certain criteria of RICH particle identification. However, by improving the RICH particle-identification software a better separation between π and K can be achieved at higher momenta. For the present analysis, the polar angle θ of the Cherenkov photon rings is corrected by a Neural Networks (NN) parametrisation, which intends to improve the internal description of the RICH sub-structure with respect to what was known during the original data production and the reconstruction. This correction depends upon various track parameters like position and angle at the RICH entrance, momentum of the particle etc. and is applied on an event-by-event basis. In the left panel of Fig. 1, we recall from our earlier analysis [12] the likelihood ratio for the K/π hypothesis in the highest momentum bin, where the separation was most challenging. In order to optimise the uncertainties of R_K , a lower limit of 1.5 was used there. Using in the present analysis the NN method, the separation of kaons and pions is improved considerably as illustrated in the right panel of Fig. 1, where the θ distribution after the NN correction is shown for the same events as in the left panel. A much better separation of the two particle species is clearly visible, which allows us to extend the analysis to higher momenta up to 55 GeV/c .

In order to obtain the raw kaon yield, the spectra as the one shown in the right panel of Fig. 1 are fitted in each z and p_h bin using the functional form described below. It turns out that a single Gaussian to describe the kaon peak and two Gaussians for the pion peak are sufficient to obtain the raw kaon yield. The fit is performed simultaneously in all z and p_h bins. This procedure is

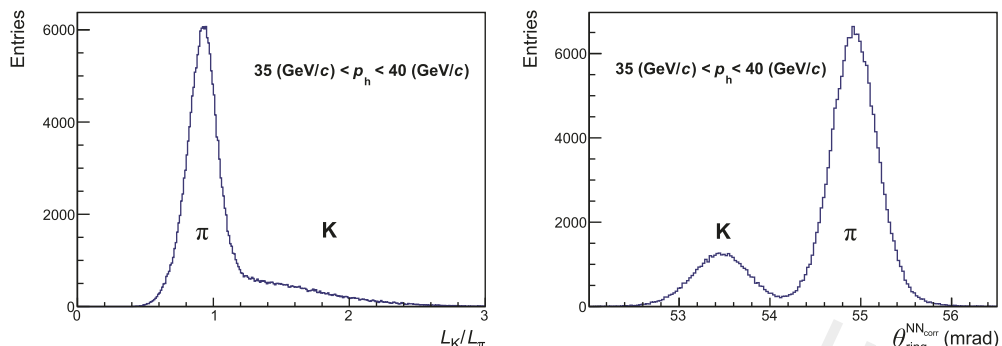


Fig. 1. Left panel: RICH likelihood ratio of K over π hypotheses for tracks with momenta between 35 GeV/c and 40 GeV/c where the separation between K and π is not obvious. In order to select kaons, the constraint $L_K/L_\pi > 1.5$ was used in Ref. [12]. Right panel: reconstructed angle of Cherenkov photons in the “ring fit” after the NN correction (which is used in the present analysis), for the same experimental data as shown in the left panel. Here, a much cleaner separation between K and π is visible.

a source of non-negligible systematic uncertainties, especially at higher z and higher momenta. The systematic uncertainty related to this extraction is described in Section 5. It is verified that the results obtained with the new method agree in the overlapping kinematic region with those previously published [12]. Hence, whenever possible, already published results on R_K are used throughout the present paper, while the new results on R_K are only given for the newly explored kaon momentum range between 40 GeV/c and 55 GeV/c.

5. Studies of systematic uncertainties

This section is split into two parts. In the first part, studies of systematic effects for the proton results are described. This is a rather standard analysis that benefits from the significant knowledge acquired with the previously published COMPASS analyses [9,10,12]. In the second part, the kaon results are described. As for the first time in COMPASS a new method is used to estimate the kaon yield, detailed studies are performed to verify the reliability of the results. Additionally, standard studies as done for R_K in Ref. [12] are also performed.

5.1. Systematic uncertainties for R_p

The COMPASS data taking was divided into periods, mainly depending upon the schedule of the SPS accelerator. A typical data period took about one week, and in between two periods interventions to the COMPASS spectrometer could happen. The whole 2006 data taking took about half a year. Therefore, it is verified that the values for R_p obtained from different data periods agree with one another. As in Ref. [12], and contrary to standard multiplicity analyses [9–11], two trigger types are used in this analysis, with or without the requirement of energy deposit in the calorimeters. It is verified that these two trigger types give consistent values for R_p . This result is expected as for the lowest proton energy analysed (20 GeV) calorimeter efficiencies are already close to 100%. More complex methods of unfolding the acceptance were tested in Ref. [12], as well as in the present analysis. They are giving very similar results when compared to the selected method, but their resulting covariance matrix has large off-diagonal elements. On the contrary, for the selected method the results in each bin and their statistical uncertainties can be considered to be independent from each other.

i) The key correction factor that has to be applied to the raw value of R_p is the acceptance difference between p and \bar{p} . The COMPASS spectrometer is charge symmetric at the level of 1%. However, protons and anti-protons interact differently with the target material as they do not have the same re-interaction length in the long solid-state COMPASS ${}^6\text{LiD}$ target. Therefore, as already

mentioned in Sect. 4, the acceptance for \bar{p} is about 10% lower than that for p, with an estimated uncertainty of about 3%.

ii) A correction factor has to be taken into account because of possibly different RICH reconstruction efficiencies for p and \bar{p} . While the correction factor is found to be one, the systematic studies suggest that its uncertainty is about 5%. This uncertainty on R_p is by 2% larger than that found for R_K , mostly due to the higher mass of the proton compared to that of the kaon, which leads to less photons per ring in the RICH in most of the phase space region covered. On top of that, some performed tests are limited in precision due to the small statistics, especially for anti-protons at larger momenta and/or larger values of z .

iii) As in previous studies, the stability of R_p is tested on data using several variables that are defined in the spectrometer coordinate system. A clear instability is seen in the dependence of R_p upon the azimuthal angle measured in the laboratory frame, as it was the case in our earlier analysis of R_K . In Ref. [12], this asymmetry led to a systematic uncertainty of up to 12% in both x -bins. In this analysis, for data binned in x and z , the systematic uncertainty amounts up to 5% for the 1st x -bin and up to 11% in the 2nd x -bin. For data binned in z and p_h , it can be up to 15% for high momenta. Thus in a significant part of the phase space this systematic uncertainty is the dominant one.

The total systematic uncertainty of R_p is obtained by adding in quadrature the above discussed three contributions. The relative systematic uncertainty is found to range between 6% and 16%. The correlation between systematic uncertainties in various z and p_h -bins is about 0.7–0.8, as in Ref. [12].

5.2. Systematic uncertainties for R_K

Most studies of systematic effects for kaon results follow closely the ones from Ref. [12], which are also described above for protons.

i) The systematic uncertainty related to the acceptance ratio and the RICH efficiency ratio for the two kaon charges is taken as in Ref. [12], i.e. 2% and 3%, respectively.

ii) The uncertainty related to the azimuthal-angle distribution of hadrons in the spectrometer is studied using the same method as in our previous paper and the resulting relative uncertainty ranges between 4% and 12%.

iii) Compared to the analysis presented in Ref. [12], a new type of systematic uncertainty has to be studied, which is related to the new method of extracting the raw kaon yields from RICH data. First, it is verified that the results obtained with the new method do agree with those previously published [12]. Various combinations of functional forms are used in the fit, e.g. the main results are obtained using a Gaussian functional form to fit the polar angle distribution of the kaon and two Gaussian functions for the one of the pion. With three Gaussian functions to describe the po-

lar angle distribution of photons in the RICH detector, there are nine free parameters in every single z and hadron momentum bin, and for each of the two hadron charges. The fit in certain bins (at large z and large momentum) results in very large uncertainties on the obtained values of R_K . In order to improve accuracy, studies are performed to determine which parameters can be kept common for the two charges and across various z and momentum bins. For example, the pion and kaon Cherenkov opening angles depend only on the particle momenta but not on z . Indeed, it is confirmed in the fit that this angle is independent on z within uncertainties. Altogether, the initial 450 free parameters in the fit are reduced by about a factor of three. The systematic uncertainty of the final results on R_K is evaluated by performing several fits, in which the number of free parameters is increased by releasing certain constraints. As a systematic uncertainty, half of the difference between maximum and minimum value of R_K obtained in these studies is taken. The resulting relative uncertainty of the kaon yield is found to range between 4% and 25%.

The total systematic uncertainty of R_K is found to range between 7% and 28% of the R_K value, and correspondingly between 0.4 and 1.1 of the statistical uncertainty on R_K . As in previous analyses, the correlation between systematic uncertainties in various z and p_h -bins is about 0.7–0.8. We note that since in the fit certain parameters are kept to be the same for various z and p_h -bins correlations may be introduced between R_K values extracted in different bins. These correlations are found to be below 5% and hence neglected.

6. Results and discussion

In Fig. 2 and Table 1, the results on the anti-proton over proton multiplicity ratio R_p are presented as a function of the variable z_{corr} for the two x -bins used in this analysis. The insert of the figure shows the “double ratio” $D_p = R_p(x < 0.05)/R_p(x > 0.05)$ that may be considered constant within uncertainties over the full measured z -range, with an average value of $D_p = 1.62 \pm 0.04_{\text{stat.}} \pm 0.07_{\text{syst.}}$. The most important observation is that with the increase of z the measured value of R_p is increasingly undershooting the LO pQCD expectation, which is 0.51 and 0.28 calculated for the average kinematics of the data in the 1st and 2nd x -bin, respectively. It is remarkable that R_p falls below the LO pQCD prediction over the whole measured z range, which starts in this analysis from $z > 0.5$. This effect was observed for R_K only for $z > 0.8$. We note that the measured z -dependence of R_p can be fitted in both x -bins by simple functional forms, e.g. $\propto (1 - z)^\beta$. The obtained β

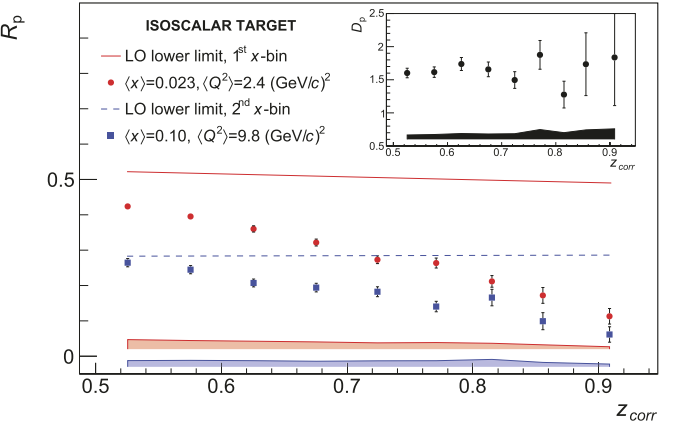


Fig. 2. Results on R_p as a function of z_{corr} for the two x -bins. The insert shows the double ratio D_p defined as the ratio of R_p in the first x -bin over R_p in the second x -bin. Statistical uncertainties are shown by error bars and systematic uncertainties by shaded bands at the bottom. The lines indicate the lower limit on R_p predicted by LO pQCD using the PDF set from Ref. [17]. The relative uncertainty of the limit is below 4% in both x -bins.

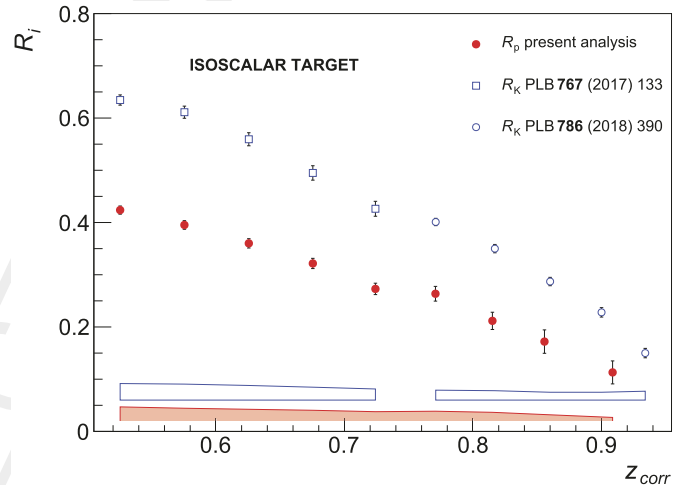


Fig. 3. Results on R_p and R_K as a function of z_{corr} for the first x -bin, $x < 0.05$. The ratio R_p falls below R_K in the whole measured phase space. The kaon data come from Refs. [10,12]. Statistical uncertainties are shown by error bars, systematic uncertainties by the bands at the bottom.

Table 1

Extracted values of R_p with statistical and systematic uncertainties, bin limits of z ($z_{\text{min}}, z_{\text{max}}$), and average values of x , Q^2 , z_{rec} and z_{corr} in the first (upper part) and second (lower part) x -bin.

Bin	x	Q^2 (GeV/c) 2	z_{min}	z_{max}	z_{rec}	z_{corr}	$R_p \pm \delta R_p, \text{stat.} \pm \delta R_p, \text{syst.}$
1	0.021	2.4	0.50	0.55	0.524	0.524	$0.4238 \pm 0.0078 \pm 0.0270$
2	0.022	2.2	0.55	0.60	0.575	0.575	$0.3953 \pm 0.0082 \pm 0.0244$
3	0.022	2.1	0.60	0.65	0.624	0.624	$0.3601 \pm 0.0089 \pm 0.0224$
4	0.023	2.0	0.65	0.70	0.675	0.675	$0.3216 \pm 0.0098 \pm 0.0205$
5	0.024	1.9	0.70	0.75	0.724	0.724	$0.2729 \pm 0.0109 \pm 0.0178$
6	0.025	1.8	0.75	0.80	0.775	0.774	$0.2636 \pm 0.0141 \pm 0.0187$
7	0.026	1.8	0.80	0.85	0.826	0.820	$0.2117 \pm 0.0165 \pm 0.0166$
8	0.026	1.7	0.85	0.90	0.878	0.865	$0.1720 \pm 0.0224 \pm 0.0123$
9	0.028	1.7	0.90	1.10	0.948	0.915	$0.1130 \pm 0.0220 \pm 0.0068$
1'	0.100	10.5	0.50	0.55	0.525	0.525	$0.2646 \pm 0.0117 \pm 0.0176$
2'	0.101	9.7	0.55	0.60	0.575	0.575	$0.2448 \pm 0.0116 \pm 0.0183$
3'	0.101	9.0	0.60	0.65	0.625	0.625	$0.2072 \pm 0.0111 \pm 0.0174$
4'	0.101	8.4	0.65	0.70	0.675	0.675	$0.1941 \pm 0.0122 \pm 0.0158$
5'	0.100	7.8	0.70	0.75	0.725	0.725	$0.1824 \pm 0.0140 \pm 0.0170$
6'	0.102	7.5	0.75	0.80	0.774	0.771	$0.1405 \pm 0.0148 \pm 0.0173$
7'	0.102	7.1	0.80	0.85	0.823	0.815	$0.1659 \pm 0.0233 \pm 0.0210$
8'	0.099	6.4	0.85	0.90	0.872	0.855	$0.0991 \pm 0.0241 \pm 0.0125$
9'	0.104	5.9	0.90	1.10	0.948	0.910	$0.0615 \pm 0.0218 \pm 0.0078$

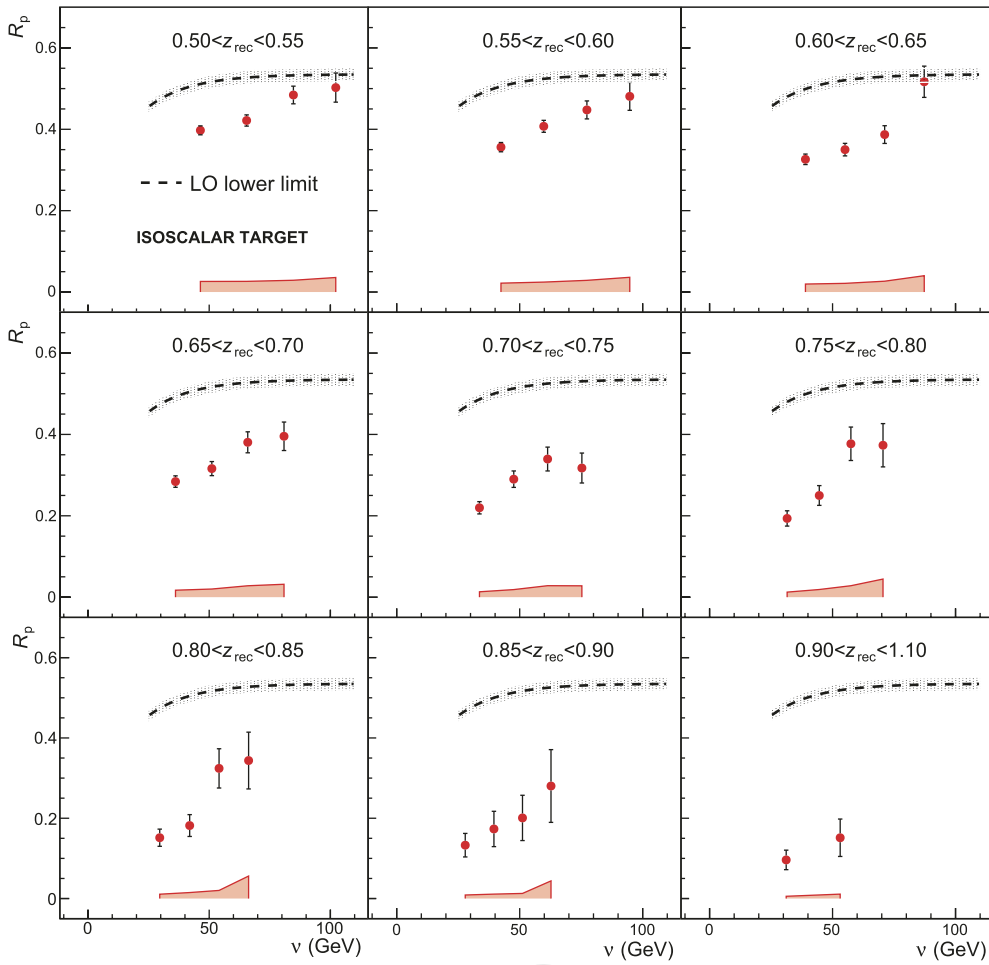


Fig. 4. Results on R_p as a function of v in nine bins of z_{rec} for the first x -bin, $x < 0.05$. Statistical uncertainties are shown by error bars, systematic uncertainties by the shaded bands at the bottom. The dashed curve, which is the same in all z -bins, represents the lower limit for R_p calculated in LO pQCD using the PDF set of Ref. [17]. The shaded band around the LO lower limit indicates its uncertainty.

value for this fit, $\beta = 0.75 \pm 0.04$, agrees within uncertainties well with $\beta = 0.71 \pm 0.03$ obtained from the fit to R_K in Ref. [12]. As β depends on the momentum range used for the analysis, its value appears only to be a reflection of the R_K and R_p dependence upon the missing mass M_X , which is discussed below.

In Fig. 3, the comparison of R_p with R_K calculated using data from Refs. [10] and [12] shows that over the whole measured phase space R_p falls significantly below R_K . Using in the proton analysis the MSTW08L PDF set [17] and the DSS FF set [5], at average values of x and Q^2 the ratio R_K/R_p is expected to be about 1.10 ± 0.05 in LO pQCD.² As mentioned above, the x and Q^2 distributions from the proton and kaon analyses are different, which turns out to reduce the expected value of the R_K/R_p ratio by about 5% to 10%. Thus in LO pQCD one would expect the proton and kaon data points shown in Fig. 3 to agree within better than 5%, which is clearly not the case.

One of the striking features of the observed disagreement between the expectation of (N)LO pQCD and the results on R_K obtained in Ref. [12] was the observed strong dependence of R_K on the virtual-photon energy v , with values of R_K closer to the pQCD prediction for higher v . Our present results on R_p do confirm a similar dependence for the proton case. These results as well as

² The quoted uncertainty includes not only the ones given by MSTW08L and DSS sets but also accounts for changes in R_K/R_p in case other PDFs and FFs sets are considered, e.g. [6,18,19].

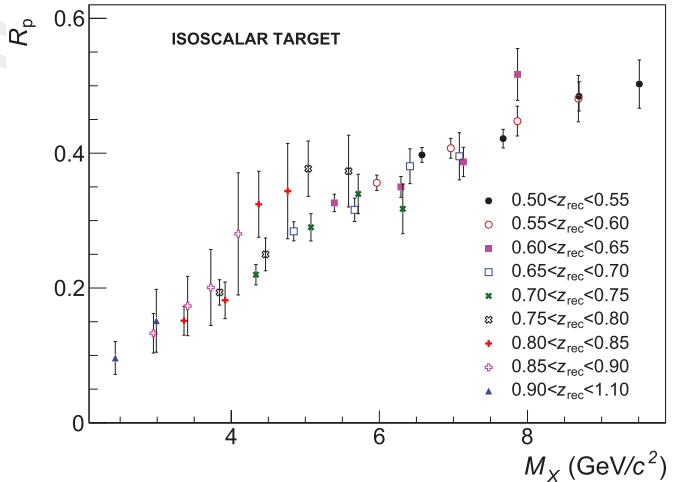


Fig. 5. Results on R_p as a function of missing mass M_X for the first x -bin, $x < 0.05$. For clarity only statistical uncertainties are shown.

the prediction of LO pQCD are shown in Fig. 4 and in Table 2. Much higher energies than those available in COMPASS seem to be required to eventually reach in the high- z region the lower limit of R_p predicted by LO pQCD. We mention that the lower limit of R_p does not directly depend on v . The v -dependence of the pQCD

Table 2

Extracted values of R_p with statistical and systematic uncertainties, bin range of proton momenta (p_{rg} (GeV/c)), bin range in z (z_{rg}), and average values of x , Q^2 , z_{rec} and z_{corr} in the first x -bin.

Bin	x	Q^2 (GeV/c) 2	p_{rg} (GeV/c)	z_{rg}	z_{rec}	z_{corr}	$R_p \pm \delta R_{p, stat.} \pm \delta R_{p, syst.}$
1a	0.022	1.9	20–30	0.50–0.55	0.524	0.524	$0.3973 \pm 0.0110 \pm 0.0260$
1b	0.020	2.5	30–40	0.50–0.55	0.525	0.525	$0.4215 \pm 0.0138 \pm 0.0262$
1c	0.020	3.2	40–50	0.50–0.55	0.524	0.524	$0.4843 \pm 0.0217 \pm 0.0289$
1d	0.021	4.0	50–60	0.50–0.55	0.526	0.526	$0.5024 \pm 0.0358 \pm 0.0357$
2a	0.023	1.9	20–30	0.55–0.60	0.575	0.575	$0.3561 \pm 0.0114 \pm 0.0218$
2b	0.020	2.3	30–40	0.55–0.60	0.574	0.574	$0.4073 \pm 0.0147 \pm 0.0244$
2c	0.020	3.0	40–50	0.55–0.60	0.575	0.575	$0.4476 \pm 0.0221 \pm 0.0287$
2d	0.020	3.6	50–60	0.55–0.60	0.575	0.575	$0.4808 \pm 0.0343 \pm 0.0362$
3a	0.024	1.8	20–30	0.60–0.65	0.624	0.624	$0.3262 \pm 0.0129 \pm 0.0196$
3b	0.021	2.1	30–40	0.60–0.65	0.625	0.625	$0.3499 \pm 0.0154 \pm 0.0213$
3c	0.020	2.7	40–50	0.60–0.65	0.624	0.624	$0.3870 \pm 0.0218 \pm 0.0266$
3d	0.020	3.3	50–60	0.60–0.65	0.624	0.624	$0.5167 \pm 0.0384 \pm 0.0401$
4a	0.026	1.7	20–30	0.65–0.70	0.675	0.675	$0.2840 \pm 0.0141 \pm 0.0171$
4b	0.021	2.0	30–40	0.65–0.70	0.675	0.675	$0.3160 \pm 0.0173 \pm 0.0200$
4c	0.020	2.5	40–50	0.65–0.70	0.675	0.675	$0.3806 \pm 0.0258 \pm 0.0280$
4d	0.020	3.1	50–60	0.65–0.70	0.675	0.675	$0.3954 \pm 0.0350 \pm 0.0317$
5a	0.027	1.7	20–30	0.70–0.75	0.724	0.724	$0.2197 \pm 0.0151 \pm 0.0132$
5b	0.022	1.9	30–40	0.70–0.75	0.724	0.724	$0.2899 \pm 0.0202 \pm 0.0186$
5c	0.020	2.3	40–50	0.70–0.75	0.725	0.725	$0.3395 \pm 0.0293 \pm 0.0282$
5d	0.020	2.9	50–60	0.70–0.75	0.724	0.724	$0.3174 \pm 0.0368 \pm 0.0279$
6a	0.028	1.6	20–30	0.75–0.80	0.776	0.773	$0.1935 \pm 0.0188 \pm 0.0124$
6b	0.022	1.9	30–40	0.75–0.80	0.775	0.774	$0.2499 \pm 0.0243 \pm 0.0188$
6c	0.020	2.2	40–50	0.75–0.80	0.774	0.774	$0.3770 \pm 0.0411 \pm 0.0281$
6d	0.020	2.7	50–60	0.75–0.80	0.774	0.773	$0.3734 \pm 0.0532 \pm 0.0445$
7a	0.029	1.6	20–30	0.80–0.85	0.827	0.819	$0.1515 \pm 0.0214 \pm 0.0108$
7b	0.023	1.8	30–40	0.80–0.85	0.824	0.819	$0.1818 \pm 0.0272 \pm 0.0149$
7c	0.020	2.1	40–50	0.80–0.85	0.824	0.821	$0.3242 \pm 0.0489 \pm 0.0202$
7d	0.020	2.5	50–60	0.80–0.85	0.823	0.820	$0.3437 \pm 0.0707 \pm 0.0560$
8a	0.030	1.5	20–30	0.85–0.90	0.882	0.866	$0.1329 \pm 0.0293 \pm 0.0088$
8b	0.024	1.8	30–40	0.85–0.90	0.875	0.862	$0.1733 \pm 0.0440 \pm 0.0124$
8c	0.020	2.0	40–50	0.85–0.90	0.874	0.865	$0.2008 \pm 0.0564 \pm 0.0127$
8d	0.020	2.3	50–60	0.85–0.90	0.872	0.865	$0.2802 \pm 0.0906 \pm 0.0437$
9ab	0.031	1.5	20–40	0.90–1.10	0.954	0.917	$0.0958 \pm 0.0242 \pm 0.0057$
9cd	0.022	2.0	40–60	0.90–1.10	0.936	0.910	$0.1466 \pm 0.0451 \pm 0.0099$

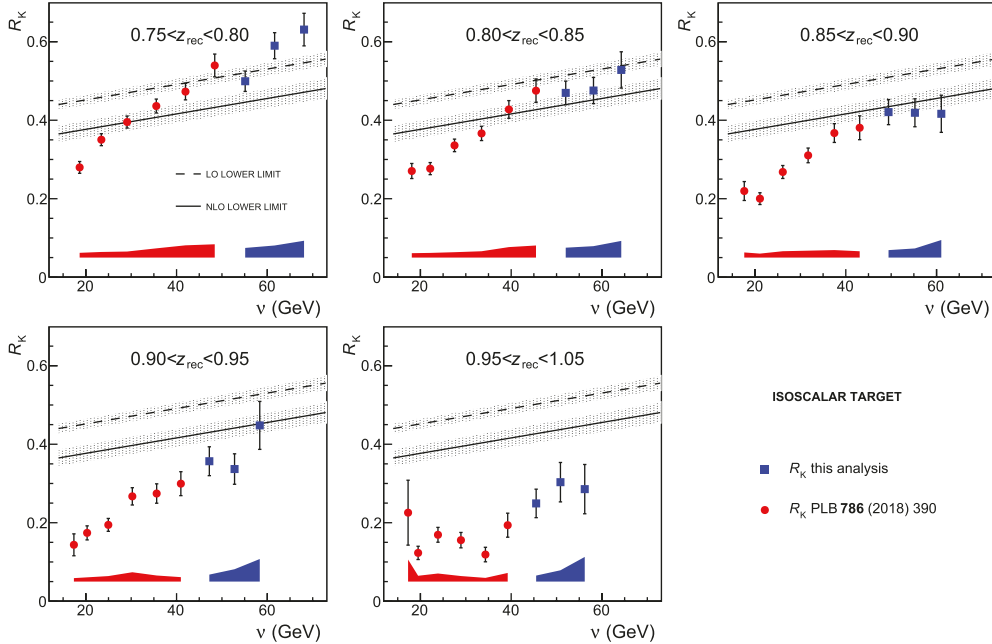


Fig. 6. The K^- over K^+ multiplicity ratio as a function of v in five bins of z obtained in this analysis (blue) and in Ref. [12] (red). The errors bars represent statistical uncertainties. The systematic uncertainties of the data points are indicated by the shaded band at the bottom of each panel. The shaded bands around the (N)LO lower limits indicate their uncertainties.

Table 3

Extracted values of R_K with statistical and systematic uncertainties, bin range of kaon momenta (p_{rg} (GeV/c)), bin range in z (z_{rg}), and average values of x , Q^2 , z_{rec} and z_{corr} .

Bin	x	Q^2 (GeV/c) 2	p_{rg} (GeV/c)	z_{rg}	z_{rec}	z_{corr}	$R_K \pm \delta R_{K, stat.} \pm \delta R_{K, syst.}$
1g	0.021	2.1	40–45	0.75–0.80	0.774	0.774	$0.4994 \pm 0.0260 \pm 0.0246$
1h	0.020	2.3	45–50	0.75–0.80	0.774	0.774	$0.5899 \pm 0.0332 \pm 0.0308$
1i	0.019	2.4	50–55	0.75–0.80	0.774	0.774	$0.6310 \pm 0.0415 \pm 0.0429$
2g	0.022	2.1	40–45	0.80–0.85	0.824	0.822	$0.4697 \pm 0.0300 \pm 0.0252$
2h	0.020	2.2	45–50	0.80–0.85	0.823	0.822	$0.4757 \pm 0.0334 \pm 0.0291$
2i	0.019	2.3	50–55	0.80–0.85	0.823	0.822	$0.5282 \pm 0.0462 \pm 0.0425$
3g	0.022	2.0	40–45	0.85–0.90	0.872	0.868	$0.4207 \pm 0.0320 \pm 0.0190$
3h	0.021	2.1	45–50	0.85–0.90	0.873	0.869	$0.4190 \pm 0.0356 \pm 0.0233$
3i	0.020	2.2	50–55	0.85–0.90	0.872	0.869	$0.4164 \pm 0.0473 \pm 0.0448$
4g	0.022	1.9	40–45	0.90–0.95	0.921	0.911	$0.3567 \pm 0.0368 \pm 0.0178$
4h	0.021	2.1	45–50	0.90–0.95	0.921	0.911	$0.3368 \pm 0.0388 \pm 0.0315$
4i	0.020	2.2	50–55	0.90–0.95	0.921	0.913	$0.4480 \pm 0.0611 \pm 0.0575$
5g	0.023	1.9	40–45	0.95–1.05	0.974	0.945	$0.2492 \pm 0.0363 \pm 0.0153$
5h	0.022	2.0	45–50	0.95–1.05	0.975	0.952	$0.3033 \pm 0.0502 \pm 0.0288$
5i	0.020	2.1	50–55	0.95–1.05	0.974	0.952	$0.2856 \pm 0.0628 \pm 0.0628$

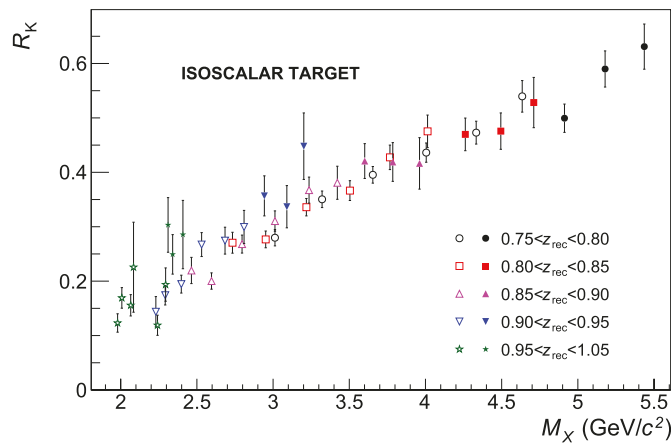


Fig. 7. The K^- over K^+ multiplicity ratio presented as a function of M_X for this analysis (full symbols) and for the analysis in Ref. [12] (open symbols), see text for details. For clarity only statistical uncertainties are shown.

lower limit seen in Fig. 4 is related to different values of x and Q^2 for different values of ν .

In Ref. [12] it was found that the z and ν dependences, which are both unexpected in pQCD, can be combined in the dependence on only one observable, which is the missing mass in the final state that is approximately given by $M_X = \sqrt{M_p^2 + 2M_p\nu(1-z) - Q^2(1-z)^2}$. In Fig. 5 the antiproton over proton multiplicity ratio R_p is shown as a function of the missing mass, and indeed a smooth trend with overlapping points at different values of z is observed.

The strong ν dependence of R_K discussed above, as originally seen in Ref. [12], was also the inspiration to extend the covered ν range by improving the RICH K - π separation. In this way, kaon identification up to 55 GeV/c was achieved instead of 40 GeV/c previously, which allows us to extend the covered ν range in every z bin. In Fig. 6, the obtained results of R_K in bins of z as a function of ν in the extended momentum range are compared to the ones published in Ref. [12], as well as to the NLO pQCD lower limit for R_K . The results confirm that the compatibility with pQCD expectations is better at higher ν . They also suggest that with increasing values of ν the growth of the ratio R_K becomes smaller. These results are also given in Table 3.

For completeness, in Fig. 7 the values of R_K in the extended momentum range are compared to our earlier results [12] as a function of missing mass. The smooth growth with M_X is still seen

over the full kinematically accessible range. Now there is larger overlap in M_X between different z -bins, i.e. one can find M_X regions where in four different z bins at very different values of ν the results on R_K are found to be consistent with one another.

7. Summary

In this article the \bar{p} over p multiplicity ratio R_p , obtained from semi-inclusive measurements of deep-inelastic lepton-nucleon scattering at z -values above 0.5, is presented for the first time. In the whole studied z -region the ratio R_p is observed to be below the lower limit predicted by LO pQCD. It is found to be significantly smaller than the K^- over K^+ multiplicity ratio R_K as presented in our previous Letter, while in LO pQCD both ratios are expected to be very similar. A strong dependence on the virtual-photon energy ν is observed, which is also not expected by LO pQCD but was already seen for the ratio R_K in our earlier analysis. The results of the proton analysis are compared to the prediction of LO pQCD. However, based on the experience with kaons it is unlikely that higher-order corrections alone will allow one to reconcile the presented proton results with pQCD predictions. In this article, the analysis of R_K is extended to larger values of ν up to 70 GeV. The obtained results suggest that for high ν values there is an indication for saturation of R_K at or above the value predicted by the NLO pQCD lower limit. The presented results of both analyses strengthen our earlier conclusion that at COMPASS energies the phase space available for single-hadron production in deep-inelastic scattering should be taken into account in the standard pQCD formalism. When using this approach, factorisation in the current-fragmentation region should work better at high z , opposite to the trend visible in our data. We hence hope that our results will evoke greater attention of theorists to the validation of the factorisation theorem for the SIDIS cross section at moderate energies.

Declaration of competing interest

The authors declare that they have no known competing financial interests or personal relationships that could have appeared to influence the work reported in this paper.

Acknowledgements

We gratefully acknowledge the support of the CERN management and staff and the skill and effort of the technicians of our

1 collaborating institutes. This work was made possible by the financial support of our funding agencies.

4 References

[1] V.N. Gribov, L.N. Lipatov, Sov. J. Nucl. Phys. 15 (1972) 438; L.N. Lipatov, Sov. J. Nucl. Phys. 20 (1975) 95; G. Altarelli, G. Parisi, Nucl. Phys. B 126 (1977) 298; Yu.L. Dokshitzer, Sov. Phys. JETP 46 (1977) 641.

[2] M. Hirai, S. Kumano, T.-H. Nagai, K. Sudoh, Phys. Rev. D 75 (2007) 094009.

[3] M. Hirai, H. Kawamura, S. Kumano, K. Saito, Prog. Theor. Exp. Phys. 2016 (2016) 113B04.

[4] N. Sato, et al., Phys. Rev. D 94 (2016) 114004.

[5] D. de Florian, R. Sassot, M. Stratmann, Phys. Rev. D 75 (2007) 114010.

[6] D. de Florian, et al., Phys. Rev. D 95 (2017) 094019.

[7] NNPDF Collaboration, V. Bertone, et al., Eur. Phys. J. C 77 (2017) 516.

[8] HERMES Collaboration, A. Airapetian, et al., Phys. Rev. D 87 (2013) 074029.

[9] COMPASS Collaboration, C. Adolph, et al., Phys. Lett. B 764 (2017) 1.

[10] COMPASS Collaboration, C. Adolph, et al., Phys. Lett. B 767 (2017) 133.

[11] COMPASS Collaboration, M. Aghasyan, et al., Phys. Rev. D 97 (2018) 032006.

[12] COMPASS Collaboration, R. Akhunzhanov, et al., Phys. Lett. B 786 (2018) 390.

[13] M. Anselmino, et al., Phys. Rev. D 71 (2005) 074006.

[14] W. Furmanski, R. Petronzio, Z. Phys. C 11 (1982) 293.

[15] D. de Florian, M. Stratmann, W. Vogelsang, Phys. Rev. D 57 (1998) 5811.

[16] R. Jakob, P.J. Mulders, J. Rodrigues, Nucl. Phys. A 626 (1997) 937.

[17] A.D. Martin, W.J. Stirling, R.S. Thorne, G. Watt, Eur. Phys. J. C 64 (2009) 653.

[18] L.A. Harland-Lang, A.D. Martin, P. Motylinski, R.S. Thorne, Eur. Phys. J. C 75 (2015) 204.

[19] NNPDF Collaboration, R.D. Ball, et al., J. High Energy Phys. 04 (2015) 040.

[20] G. Ingelman, A. Edin, J. Rathsman, Comput. Phys. Commun. 101 (1997) 108.

[21] T. Sjöstrand, LU-TP-95-20, CERN-TH-7112-93-REV, arXiv:hep-ph/9508391.

[22] A. Kotzinian, Eur. Phys. J. C 44 (2005) 211.

[23] J.V. Guerrero, et al., J. High Energy Phys. 09 (2015) 169.

[24] E. Christova, E. Leader, Phys. Rev. D 94 (2016) 096001.

[25] J.V. Guerrero, A. Accardi, Phys. Rev. D 97 (2018) 114012.

[26] D.P. Anderle, F. Ringer, W. Vogelsang, Phys. Rev. D 87 (2013) 034014.

[27] D.P. Anderle, M. Stratmann, F. Ringer, Phys. Rev. D 92 (2015) 114017.

[28] D.P. Anderle, T. Kaufmann, M. Stratmann, F. Ringer, Phys. Rev. D 95 (2017) 054003.

[29] M. Epele, C.G. Canal, R. Sassot, Phys. Rev. D 94 (2016) 034037.

[30] M. Epele, C.G. Canal, R. Sassot, Phys. Lett. B 790 (2019) 102.

[31] A. Accardi, A. Signori, Phys. Lett. B 798 (2019) 134993.

[32] COMPASS Collaboration, P. Abbon, et al., Nucl. Instrum. Methods 577 (2007) 455.

[33] P. Abbon, et al., Nucl. Instrum. Methods A 631 (2011) 26.

[34] E.C. Aschenauer, et al., Phys. Rev. D 88 (2013) 114025; H. Spiesberger HERACLES, DJANGOH, Event Generation of ep Interactions at HERA Including Radiative Processes, (version 1.6).

23 The COMPASS Collaboration

M.G. Alexeev ^{y,z}, G.D. Alexeev ^g, A. Amoroso ^{y,z}, V. Andrieux ^{i,ab}, V. Anosov ^g, A. Antoshkin ^g, K. Augsten ^{g,r}, W. Augustyniak ^{ac}, C.D.R. Azevedo ^a, B. Badelek ^{ad}, F. Balestra ^{y,z}, M. Ball ^c, J. Barth ^c, R. Beck ^c, Y. Bedfer ^t, J. Berenguer Antequera ^{y,z}, J. Bernhard ^{l,i}, M. Bodlak ^q, F. Bradamante ^x, A. Bressan ^{w,x}, M. Büchele ^h, V.E. Burtsev ^{aa}, W.-C. Chang ^u, C. Chatterjee ^{w,x}, M. Chiosso ^{y,z}, A.G. Chumakov ^{aa}, S.-U. Chung ^{o,1,2}, A. Cicuttin ^{x,3}, P.M.M. Correia ^a, M.L. Crespo ^{x,3}, D. D'Agò ^{w,x}, S. Dalla Torre ^x, S.S. Dasgupta ^f, S. Dasgupta ^x, I. Denisenko ^g, O.Yu. Denisov ^{z,*}, S.V. Donskov ^s, N. Doshita ^{af}, Ch. Dreisbach ^o, W. Dünnweber ⁴, R.R. Dusaev ^{aa}, A. Efremov ^g, P.D. Eversheim ^c, P. Faccioli ^k, M. Faessler ⁴, M. Finger ^q, M. Finger jr. ^q, H. Fischer ^h, C. Franco ^k, J.M. Friedrich ^o, V. Frolov ^{g,i}, F. Gautheron ^{b,ab}, O.P. Gavrichtchouk ^g, S. Gerassimov ^{n,o}, J. Giarra ^l, I. Gnesi ^{y,z}, M. Gorzellik ^{h,5}, A. Grasso ^{y,z}, A. Gridin ^g, M. Grosse Perdekamp ^{ab}, B. Grube ^o, A. Guskov ^g, D. von Harrach ^l, R. Heitz ^{ab}, F. Herrmann ^h, N. Horikawa ^{p,6}, N. d'Hose ^t, C.-Y. Hsieh ^{u,7}, S. Huber ^o, S. Ishimoto ^{af,8}, A. Ivanov ^g, T. Iwata ^{af}, M. Jandek ^r, V. Jary ^r, R. Joosten ^c, P. Jörg ^{h,9}, E. Kabuß ^l, F. Kaspar ^o, A. Kerbizi ^{w,x}, B. Ketzer ^c, G.V. Khaustov ^s, Yu.A. Khokhlov ^{s,10}, Yu. Kisselev ^{g,11}, F. Klein ^d, J.H. Koivuniemi ^{b,ab}, V.N. Kolosov ^s, K. Kondo Horikawa ^{af}, I. Konorov ^{n,o}, V.F. Konstantinov ^s, A.M. Kotzinian ^{z,12}, O.M. Kouznetsov ^g, A. Koval ^{ac}, Z. Kral ^q, F. Krinner ^o, Y. Kulinich ^{ab}, F. Kunne ^t, K. Kurek ^{ac}, R.P. Kurjata ^{ae}, A. Kveton ^q, K. Lavickova ^r, S. Levorato ^x, Y.-S. Lian ^{u,13}, J. Lichtenstadt ^v, P.-J. Lin ^{t,14}, R. Longo ^{ab}, V.E. Lyubovitskij ^{aa,15}, A. Maggiora ^z, A. Magnon ¹⁶, N. Makins ^{ab}, N. Makke ^{x,3}, G.K. Mallot ⁱ, A. Maltsev ^g, S.A. Mamon ^{aa}, B. Marianski ^{ac,11}, A. Martin ^{w,x}, J. Marzec ^{ae}, J. Matoušek ^{w,x}, T. Matsuda ^m, G. Mattsson ^{ab}, G.V. Meshcheryakov ^g, M. Meyer ^{ab,t}, W. Meyer ^b, Yu.V. Mikhailov ^s, M. Mikhasenko ^{c,i}, E. Mitrofanov ^g, N. Mitrofanov ^g, Y. Miyachi ^{af}, A. Moretti ^{w,x}, A. Nagaytsev ^g, C. Naim ^t, D. Neyret ^t, J. Nový ^r, W.-D. Nowak ^l, G. Nukazuka ^{af}, A.S. Nunes ^{k,17}, A.G. Olshevsky ^g, M. Ostrick ^l, D. Panzieri ^{z,18}, B. Parsamyan ^{y,z}, S. Paul ^o, H. Pekeler ^c, J.-C. Peng ^{ab}, M. Pešek ^q, D.V. Peshekhonov ^g, M. Pešková ^q, N. Pierre ^{l,t}, S. Platchkov ^t, J. Pochodzalla ^l, V.A. Polyakov ^s, J. Pretz ^{d,19}, M. Quaresma ^{u,k}, C. Quintans ^k, G. Reicherz ^b, C. Riedl ^{ab}, T. Rudnicki ^{ad}, D.I. Ryabchikov ^{s,o}, A. Rybníkov ^g, A. Rychter ^{ae}, V.D. Samoylenko ^s, A. Sandacz ^{ac}, S. Sarkar ^f, I.A. Savin ^g, G. Sbrizzai ^{w,x}, H. Schmieden ^d, A. Selyunin ^g, L. Sinha ^f, M. Slunecka ^{g,q}, J. Smolik ^g, A. Srnka ^e, D. Steffen ^{i,o}, M. Stolarski ^{k,*}, O. Subrt ^{i,r}, M. Sulc ^j, H. Suzuki ^{af,6}, P. Sznajder ^{ac}, S. Tessaro ^x, F. Tessarotto ^{x,*}, A. Thiel ^c, J. Tomsa ^q, F. Tosello ^z, A. Townsend ^{ab}, V. Tskhay ⁿ, S. Uhl ^o, B.I. Vasilishin ^{aa}, A. Vauth ^{d,i,20}, B.M. Veit ^{l,i}, J. Veloso ^a, B. Ventura ^t, A. Vidon ^t, M. Virius ^r, M. Wagner ^c, S. Wallner ^o, K. Zaremba ^{ae}, P. Zavada ^g, M. Zavertyaev ⁿ, M. Zemko ^q, E. Zemlyanichkina ^g, Y. Zhao ^x, M. Ziembicki ^{ae}

^a University of Aveiro, Dept. of Physics, 3810-193 Aveiro, Portugal

^b Universität Bochum, Institut für Experimentalphysik, 44780 Bochum, Germany ^{21,22}

^c Universität Bonn, Helmholtz-Institut für Strahlen- und Kernphysik, 53115 Bonn, Germany ²¹

^d Universität Bonn, Physikalisches Institut, 53115 Bonn, Germany ²¹

^e Institute of Scientific Instruments of the CAS, 61264 Brno, Czech Republic ²³

1	^f Matrivani Institute of Experimental Research & Education, Calcutta-700 030, India	24	67
2	^g Joint Institute for Nuclear Research, 141980 Dubna, Moscow region, Russia	25	68
3	^h Universität Freiburg, Physikalisches Institut, 79104 Freiburg, Germany	21,22	69
4	ⁱ CERN, 1211 Geneva 23, Switzerland		70
5	^j Technical University in Liberec, 46117 Liberec, Czech Republic	23	71
6	^k LIP, 1649-003 Lisbon, Portugal	26	72
7	^l Universität Mainz, Institut für Kernphysik, 55099 Mainz, Germany	21	73
8	^m University of Miyazaki, Miyazaki 889-2192, Japan	27	74
9	ⁿ Lebedev Physical Institute, 119991 Moscow, Russia		75
10	^o Technische Universität München, Physik Dept., 85748 Garching, Germany	21,4	76
11	^p Nagoya University, 464 Nagoya, Japan	27	77
12	^q Charles University, Faculty of Mathematics and Physics, 12116 Prague, Czech Republic	23	78
13	^r Czech Technical University in Prague, 16636 Prague, Czech Republic		79
14	^s State Scientific Center Institute for High Energy Physics of National Research Center 'Kurchatov Institute', 142281 Protvino, Russia		80
15	^t IRFU, CEA, Université Paris-Saclay, 91191 Gif-sur-Yvette, France	22	81
16	^u Academia Sinica, Institute of Physics, Taipei 11529, Taiwan	28	82
17	^v Tel Aviv University, School of Physics and Astronomy, 69978 Tel Aviv, Israel	29	83
18	^w University of Trieste, Dept. of Physics, 34127 Trieste, Italy		84
19	^x Trieste Section of INFN, 34127 Trieste, Italy		85
20	^y University of Turin, Dept. of Physics, 10125 Turin, Italy		86
21	^z Torino Section of INFN, 10125 Turin, Italy		87
22	^{aa} Tomsk Polytechnic University, 634050 Tomsk, Russia	30	88
23	^{ab} University of Illinois at Urbana-Champaign, Dept. of Physics, Urbana, IL 61801-3080, USA	31	89
24	^{ac} National Centre for Nuclear Research, 02-093 Warsaw, Poland	32	90
25	^{ad} University of Warsaw, Faculty of Physics, 02-093 Warsaw, Poland	32	91
26	^{ae} Warsaw University of Technology, Institute of Radioelectronics, 00-665 Warsaw, Poland	32	92
27	^{af} Yamagata University, Yamagata 992-8510, Japan	27	93
28	* Corresponding authors.		94
29	E-mail addresses: oleg.denisov@cern.ch (O.Yu. Denisov), Marcin.Stolarski@cern.ch (M. Stolarski), fulvio.tessarotto@cern.ch (F. Tessarotto).		95
30	¹ Also at Dept. of Physics, Pusan National University, Busan 609-735, Republic of Korea.		96
31	² Also at Physics Dept., Brookhaven National Laboratory, Upton, NY 11973, USA.		97
32	³ Also at Abdus Salam ICTP, 34151 Trieste, Italy.		98
33	⁴ Supported by the DFG cluster of excellence 'Origin and Structure of the Universe' (www.universe-cluster.de) (Germany).		99
34	⁵ Supported by the DFG Research Training Group Programmes 1102 and 2044 (Germany).		100
35	⁶ Also at Chubu University, Kasugai, Aichi 487-8501, Japan.		101
36	⁷ Also at Dept. of Physics, National Central University, 300 Jhongda Road, Jhongli 32001, Taiwan.		102
37	⁸ Also at KEK, 1-1 Oho, Tsukuba, Ibaraki 305-0801, Japan.		103
38	⁹ Present address: Universität Bonn, Physikalisches Institut, 53115 Bonn, Germany.		104
39	¹⁰ Also at Moscow Institute of Physics and Technology, Moscow Region, 141700, Russia.		105
40	¹¹ Deceased.		106
41	¹² Also at Yerevan Physics Institute, Alikhanian Br. Street, Yerevan, Armenia, 0036.		107
42	¹³ Also at Dept. of Physics, National Kaohsiung Normal University, Kaohsiung County 824, Taiwan.		108
43	¹⁴ Supported by ANR, France with P2IO LabEx (ANR-10-LABX-0038) in the framework "Investissements d'Avenir" (ANR-11-IDEX-0003-01).		109
44	¹⁵ Also at Institut für Theoretische Physik, Universität Tübingen, 72076 Tübingen, Germany.		110
45	¹⁶ Retired.		111
46	¹⁷ Present address: Brookhaven National Laboratory, Brookhaven, USA.		112
47	¹⁸ Also at University of Eastern Piedmont, 15100 Alessandria, Italy.		113
48	¹⁹ Present address: RWTH Aachen University, III. Physikalisches Institut, 52056 Aachen, Germany.		114
49	²⁰ Present address: Universität Hamburg, 20146 Hamburg, Germany.		115
50	²¹ Supported by BMBF - Bundesministerium für Bildung und Forschung (Germany).		116
51	²² Supported by FP7, HadronPhysics3, Grant 283286 (European Union).		117
52	²³ Supported by MEYS, Grant LM20150581 (Czech Republic).		118
53	²⁴ Supported by B. Sen fund (India).		119
54	²⁵ Supported by CERN-RFBR Grant 12-02-91500.		120
55	²⁶ Supported by FCT, Grants CERN/FIS-PAR/0007/2017 and CERN/FIS-PAR/0022/2019 (Portugal).		121
56	²⁷ Supported by MEXT and JSPS, Grants 18002006, 20540299, 18540281 and 26247032, the Daiko and Yamada Foundations (Japan).		122
57	²⁸ Supported by the Ministry of Science and Technology, Taiwan.		123
58	²⁹ Supported by the Israel Academy of Sciences and Humanities (Israel).		124
59	³⁰ Supported by the Russian Federation program "Nauka" (Contract No. 0.1764.GZB.2017) (Russia).		125
60	³¹ Supported by the National Science Foundation, Grant no. PHY-1506416 (USA).		126
61	³² Supported by NCN, Grant 2017/26/M/ST2/00498 (Poland).		127
62			128
63			129
64			130
65			131
66			132